RSC Advances

PAPER

View Article Online
View Journal | View Issue

Cite this: *RSC Adv.*, 2022, **12**, 21827

Barium molybdate white emitting phosphor synthesized at room temperature by co-precipitation

Soung-Soo Yi[a] and Jae-Yong Jung *[b]

Received 24th June 2022
Accepted 22nd July 2022

DOI: 10.1039/d2ra03897h

rsc.li/rsc-advances

Crystalline $BaMoO_4:Dy^{3+}$ and $BaMoO_4:Sm^{3+}$ phosphors were synthesized by co-precipitation at room temperature. The main peak (112) phase and tetragonal structure were confirmed using X-ray diffraction analysis. The lattice constant and Raman signal on $d_{(112)}$ were changed by the rare earth doping. A strong absorption wavelength appeared in the UV region, and $BaMoO_4:Dy^{3+}$ excited with UV wavelength showed a yellow spectrum. $BaMoO_4:Sm^{3+}$ showed a reddish orange spectrum. $BaMoO_4:[Sm^{3+}]/[Dy^{3+}]$ was synthesized for use as a white light phosphor, and the change in the emission characteristics of yellow, white, and reddish orange could be observed depending on the doping concentration of Sm^{3+} ions. The synthesized phosphor powder and PDMS polymer were mixed to form a flexible composite, and when applied on a UV-LED chip, the same color as the powder was realized, suggesting its use as an LED color filter.

1. Introduction

White light emitting phosphors doped with rare earth ions are attracting research attention for various applications such as displays, lighting, and light emitting devices.[1,2] Typically, dysprosium ions are mainly used for the white light emitting phosphor. Dysprosium ions have a yellow peak (~575 nm) and a blue peak (~485 nm) when excited with ultraviolet light.[3,4] When synthesizing Dy^{3+} ions into a phosphor, the intensities of the blue and yellow light emissions are adjusted to provide a perfect white color. This adjustment is necessary because the intensities of the blue light emission from the $^4F_{9/2} \rightarrow {}^6H_{15/2}$ transition and the yellow light emission from the $^4F_{9/2} \rightarrow {}^6H_{13/2}$ transition are different, because of differences in site symmetry location, depending on the host crystal when synthesized as a phosphor.

There is another possible way to realize white light emission.[5,6] The mainstream approach to obtain white light in existing displays and light emitting devices has been to use white light emitting diodes and tricolor display devices, appropriately mixing blue, green, red, and ultraviolet wavelengths. The representative $BaMgAl_{10}O_7:Eu^{2+}$ (ref. 7) phosphor, which emits blue light, has a disadvantage in that the light emitting characteristic is deteriorated by the heat treatment process performed in oxygen atmosphere during panel manufacturing. $Zn_2SiO_4:Mn^{2+}$,[8] which is used as a green phosphor, has a problem with overlapping images because the afterimage time is too long. In the (Gd, Y)$BO_3:Eu^{3+}$ (ref. 9) red phosphor, the intensity of orange luminescence is stronger than the red, so there is some difficulty controlling color purity.

To compensate for these disadvantages, it would be useful to develop a phosphor doped with dysprosium ions that emits all colors rather than synthesizing and combining the phosphors of blue, green, and red respectively. To develop a phosphor doped with Dy^{3+} ions that has high luminous efficiency, various synthesis methods such as the solid-state reaction method,[10] sol–gel method,[11] hydrothermal method,[12] Czochralski method,[13] melt quenching method,[14] and others have been used. Raju *et al.* synthesized a $Gd_3Al_5O_{12}$ phosphor doped with Dy^{3+} ions by solvothermal synthesis and reported that the ratio of yellow and blue emission intensity was dependent on the concentration ratio of Dy^{3+} ions, and thus could be controlled.[15] Kuang *et al.* prepared a $SrSiO_3$ phosphor doped with Dy^{3+} ions using a solid-state reaction method. After irradiating the phosphor with a 254 nm ultraviolet lamp for 5 minutes and removing it, white light emission was observed for more than 1 hour. The white light emission was caused by a mixture of blue light emission at 480 nm and yellow light emission at 572 nm. Excited electrons in the electron trap site continuously transfer energy to the $^4F_{9/2}$ energy level of Dy^{3+} ions, so light emission occurs for the long time reported.[16]

Li *et al.* prepared a $NaLa(MoO_4)_2:Dy^{3+}$ phosphor with a particle size of about 1 μm with a hydrothermal method, and observed a yellow signal at 574 nm and a blue emission spectrum at 486 nm when excited at 390 nm and 456 nm. The

[a]*Division of Materials Science and Engineering, Silla University, Busan 46958, Republic of Korea*

[b]*Research and Business Development Foundation, Silla University, Engineering Building, Busan 45985, Republic of Korea. E-mail: eayoung21@naver.com; Tel: +82-51-999-6441*

maximum luminescence intensity was observed when the concentration of Dy^{3+} ions was 0.02.[17]

A case of co-doping with Sm^{3+} ions to compensate for the insufficient red color of Dy^{3+} ions was also reported for preparing white light phosphors. Fan *et al.* synthesized a warm-white light-emitting phosphor using a solid-state reaction method to co-dope Sm^{3+} and Dy^{3+} ions into a BaY_2ZnO_5 host matrix. It was observed that the color coordinates shifted from cold white to warm white depending on the doping amount of Sm^{3+} ions.[18] Yu *et al.* co-doped Sm^{3+} and Dy^{3+} ions with crystalline Sr_2SnO_4 as a host matrix and the synthesized phosphor exhibited enhanced red emission compared to a sample single doped with Dy^{3+} upon excitation at 254 nm, after being calcined at 900 °C.[19] In the present study, a barium molybdate ($BaMoO_4$) phosphor with excellent thermal and chemical stability[20] was co-doped with Dy^{3+} and Dy^{3+} and Sm^{3+} ions at room temperature by co-precipitation without additional heat treatment, an easy synthesis method. The structure and emission characteristics of the synthesized phosphor were subsequently investigated. By mixing the synthesized phosphor with a polymer to make a flexible composite, the phosphor could be used as an LED color filter.

2. Experimental

2.1. Synthesis of $BaMoO_4$ and $BaMoO_4$ phosphors by co-precipitation

Starting materials: barium acetate ($(CH_3COO)_2Ba$, Sigma-Aldrich), sodium tungstate ($Na_2MoO_4 \cdot 2H_2O$, Sigma-Aldrich), dysprosium(III) nitrate ($Dy(NO_3)_3 \cdot 5H_2O$, Dy^{3+}), and samarium(III) nitrate ($Sm(NO_3)_3 \cdot 5H_2O$, Sm^{3+}).

10 mmol of $(CH_3COO)_2Ba$ was dissolved in beaker "A" containing 100 mL of distilled water. In beaker "B", 10 mmol of $Na_2MoO_4 \cdot 2H_2O$ was dissolved in 10 mL distilled water (Fig. 1). The solution that was completely dissolved in beaker "B" was slowly poured into the stirring beaker "A" and remained there for about 20 minutes. After that, powder was recovered using a centrifuge (4000 rpm, 5 min), and the powder was prepared by rinsing with distilled water 3 times to remove any remaining sodium. The white powder was dried in an oven at 80 °C for 16 hours. The phosphor was synthesized with $BaMoO_4$ as a host, the precursor was made by simultaneously adding $Dy(NO_3)_3 \cdot 5H_2O$ and $Er(NO_3)_3 \cdot 5H_2O$ or $Sm(NO_3)_3 \cdot 5H_2O$ to beaker "A". The $BaMoO_4$:$[Sm^{3+}]/[Dy^{3+}]$ phosphor was synthesized. Rare earth [RE] ions of Dy^{3+} were fixed at 0.05 mmol, and the amount of added Sm^{3+} was changed ($[Sm^{3+}]/[Dy^{3+}] \sim 0.1, 0.2, 0.3, 0.4, 0.6, 0.8, 1$).[21]

2.2. Characterization

The crystal structure of the synthesized phosphor powder was measured using an X-ray diffraction apparatus (XRD, X'Pert PRO MPD, 40 kV, 30 mA) using Cu-Kα radiation (wavelength: 1.5406 Å) at a scan rate of 4° per minute at a diffraction angle of 10° to 70°. The size and microscopic surface shape of the crystal grains were photographed with a field emission scanning electron microscope (FE-SEM, CZ, MIRA I LMH, TESCAN), and

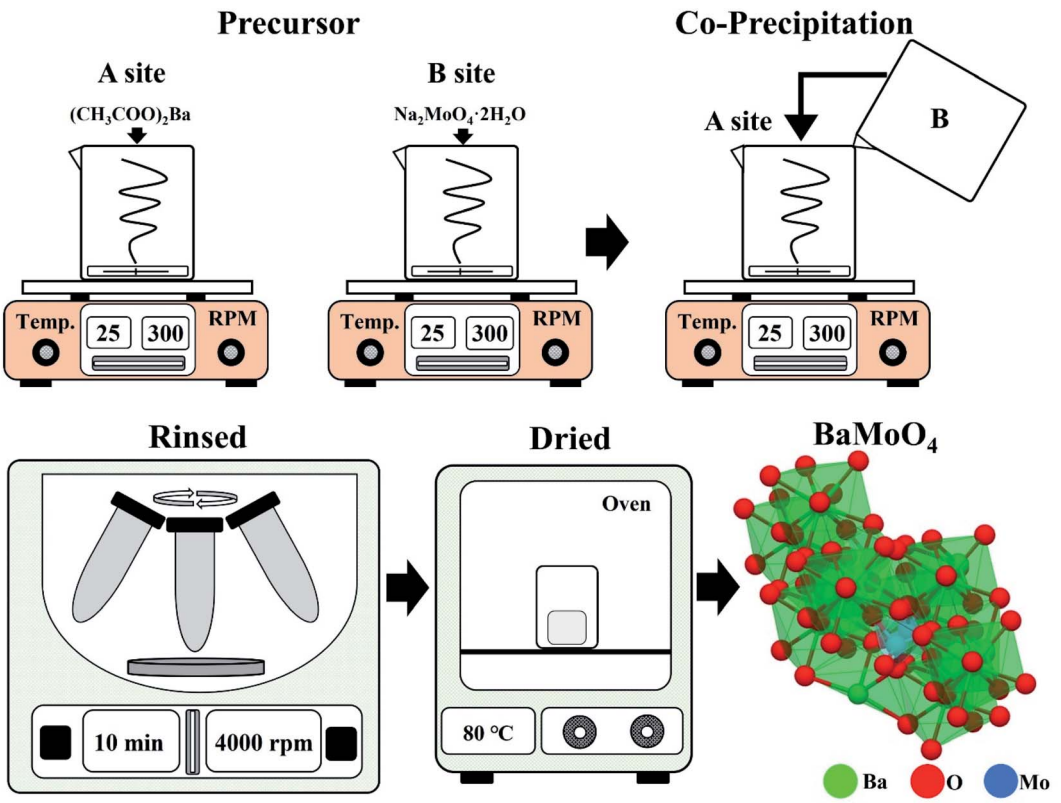

Fig. 1 Schematic of co-precipitation experimental process.

Raman spectroscope (JP/NRS-3300, 532 nm 100 mW soli-state primary laser).

2.3. Fabrication of the LED color flexible composite

The synthesized $BaMoO_4:Dy^{3+}$, $BaMoO_4:Sm^{3+}$, and $BaMoO_4$:[-Sm^{3+}]/[Dy^{3+}] ~ 0.1 phosphors were mixed at 0.1 g each with 1 g of polydimethylsiloxane (PDMS) and then cast in a square mold. After curing in an oven at 80 °C for 2 hours, the unique luminescent color was checked with a UV lamp, and the color reproducibility was checked by placing it on the LED chip.

3. Results and discussion

3.1. Characteristics of the rare earth single doped $BaMoO_4$

Fig. 2(a) shows the XRD diffraction patterns of a sample doped with crystalline $BaMoO_4$ as a host material, rare earth ions single doped $BaMoO_4:Dy^{3+}$, and $BaMoO_4:Sm^{3+}$ synthesized at room temperature, respectively. Regardless of the rare earth ions doping, the samples matched $BaMoO_4$ of ICDD no. 00-008-0455 card and had a tetragonal structure. The main peak (112) phase was strongly detected, and peaks (004), (200), (202), (114), (204), (220), (116), (312), and (224) were observed. The MXO_4 (M = Ba, Sr and Ca, X = Mo and W) nanoparticles precipitated—M^{2+} cations as electron pair acceptors (Lewis acid) and reacted with XO_4^{2-} anions as electron pair donors (Lewis base). The reaction between these two species ($M^{2+} \leftarrow :XO_4^{2-}$) resulted in bonding. The lowest molecular orbital energy of the Lewis acid interacted with the highest molecular orbital energy of the Lewis base, and MXO_4 nanoparticles were finally synthesized.[22] To investigate the changes in crystal structure due to the rare earth doping, the lattice constant was calculated using the signal position on the (112) plane, which is the main peak, and substituting it into Bragg's equation,[23] as shown in Fig. 2(b). Rare earth ions with a relatively large ionic radius were doped,[24,25] and a shift in the peak of the phase (112) was observed. The lattice constant of phase $d_{(112)}$ was increased by the rare earth ions located in the crystal lattice of $BaMoO_4$. The full width at half maximum (FWHM) of the (112) phase was also increased by doping with rare earth ions (Fig. 2(c)).

Fig. 2(d) shows the Raman shift spectrum obtained by excitation of the sample with a 532 nm laser, to observe the change in molecular frequency caused by the rare earth ions located in the doped $BaMoO_4$ crystal lattice. Raman vibration modes can be divided into two groups: external and internal modes. The first one corresponds to the motion of phonons and Ba^{2+} cations in the rigid $[MoO_4]^{2-}$ tetrahedron unit. The second belongs to $[MoO_4]^{2-}$ vibration within a tetrahedral unit, considered to be the steady state of the center.[26] The synthesized $BaMoO_4$ had frequencies of 328, 362, 793, 840, and 893 cm^{-1}. A slight change in the position of the frequencies of the $BaMoO_4:Dy^{3+}$ and $BaMoO_4:Sm^{3+}$ samples doped with rare earth ions was observed, suggesting that the vibration of

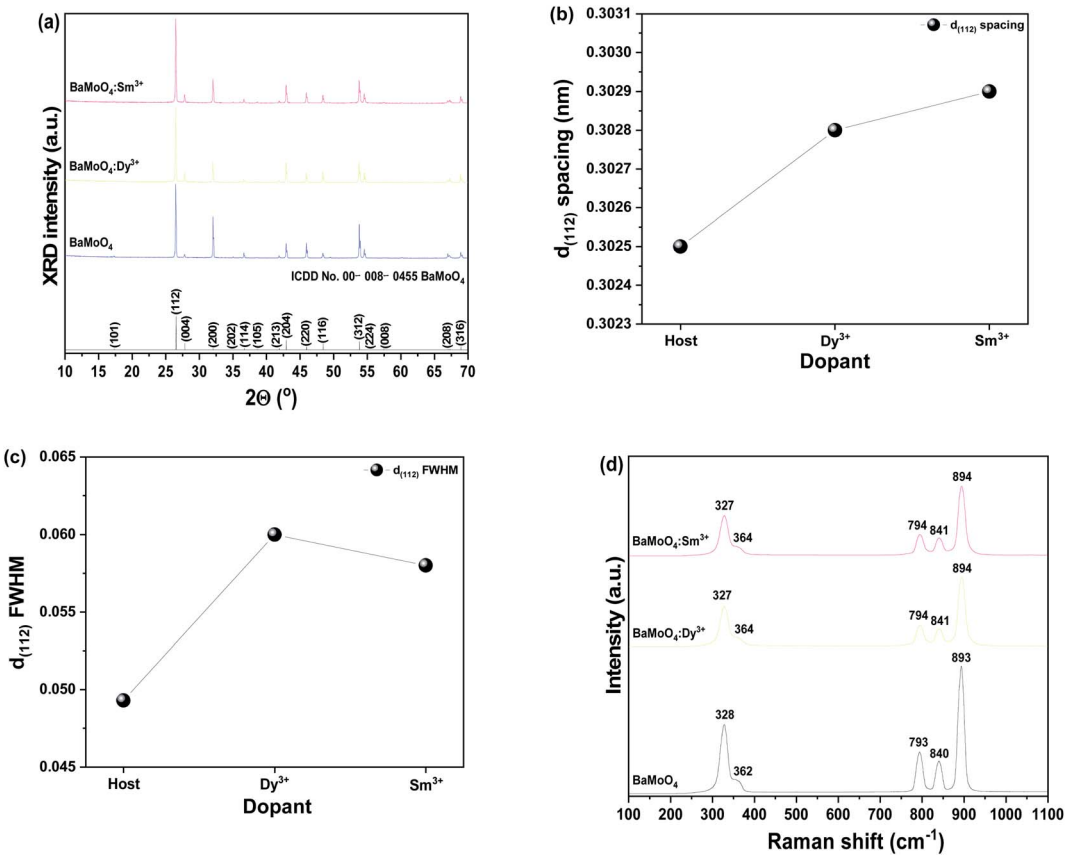

Fig. 2 (a) XRD patterns, (b) change in $d_{(112)}$ spacing, (c) change in FWHM, and (d) Raman shift of synthesized $BaMoO_4$ and $BaMoO_4:RE^{3+}$ powders.

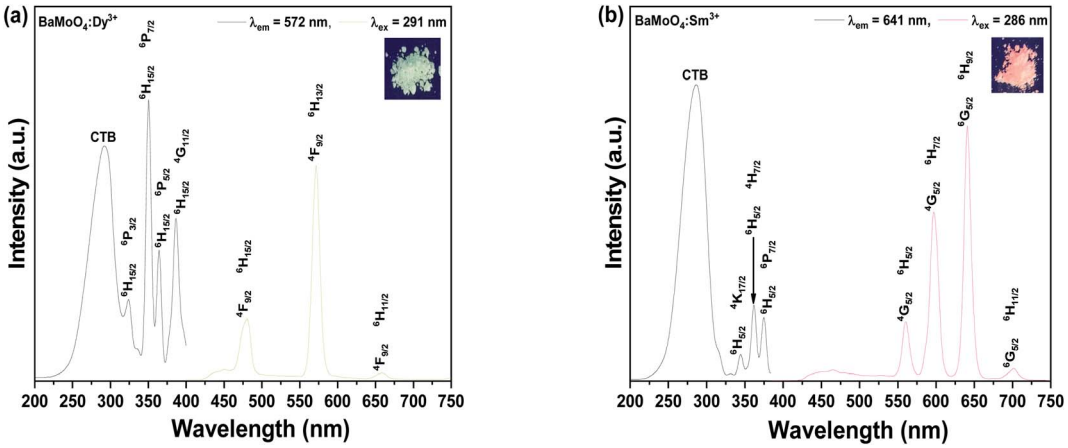

Fig. 3 Photoluminescence properties of (a) $BaMoO_4:Dy^{3+}$ and (b) $BaMoO_4:Sm^{3+}$.

molecules was affected by energy transferred from the outside by doping with rare earth ions.[27] Fig. 3 shows the spectra of the absorption and emission characteristics of the $BaMoO_4:Dy^{3+}$ and $BaMoO_4:Sm^{3+}$ phosphor powders synthesized by doping with Dy^{3+} or Sm^{3+} ions, respectively. Under the 572 nm spectrum of the $BaMoO_4:Dy^{3+}$ sample, a broad spectrum distributed over a 230–330 nm region with a peak at 291 nm were observed, as well as several narrow absorption spectra appearing in the 330–400 nm region. Absorbance with a rather wide bandwidth is a transition signal generated by a charge transfer band (CTB) between Dy^{3+} cations and O^{2-} anions, and absorbance with a narrow bandwidth is a 4*f*–4*f* transition signal generated within the $^4F_9$ electron arrangement of Dy^{3+} ions.[28] 350 nm, which was the strongest signal among the absorption peaks with a narrow bandwidth, is a signal generated while transitioning from the $^6H_{15/2}$ level, which is the ground state of the Dy^{3+} ions in the host lattice, to the $^4P_{7/2}$ energy level, which is the excited state. In contrast, wavelengths of 323 ($^6H_{15/2} \rightarrow {}^6P_{3/2}$), 351 ($^6H_{15/2} \rightarrow {}^6P_{7/2}$), 365 ($^6H_{15/2} \rightarrow {}^6P_{5/2}$), and 387 ($^6H_{15/2} \rightarrow {}^4G_{11/2}$) nm with relatively weak absorption intensity were observed. When the $BaMoO_4:Dy^{3+}$ sample was excited at 291 nm, a yellow spectrum with a strong signal at 572 nm, a blue emission spectrum with a peak at 480 nm, and a red spectrum at 659 nm with a relatively weak signal were observed. These emission signals are emission spectra resulting from the $^4F_{9/2} \rightarrow {}^6H_j$ transition of Dy^{3+} ions.[29] The yellow emission spectrum is at the $^4F_{9/2} \rightarrow {}^6H_{13/2}$ transition with $j = 13/2$, the blue emission at the $^4F_{9/2} \rightarrow {}^6H_{15/2}$ transition with $j = 15/2$, and the red emission at $j = 11/2$ known as the $^4F_{9/2} \rightarrow {}^6H_{11/2}$ transition signal.[30] It is known that the size of the emission wavelength and intensity varies depending on the degree the local environment around the rare earth ion doped in the host lattice in the phosphor is deformed in the inversion symmetry. The asymmetry ratio is defined as the ratio of the light emission intensity due to the electric dipole transition and the light emission intensity due to the magnetic dipole transition. It is known that the electric dipole transition, which generates a yellow light emission signal at 572 nm when Dy^{3+} ions are doped, belongs to a sensitive transition, and is significantly affected by the external environment of the Dy^{3+} ions. Conversely, the blue emission spectrum at 480 nm is generated by magnetic dipole transition and is hardly affected by the strength of the crystal field around the Dy^{3+} ions. That is, when blue light emission due to magnetic dipole transition is the main peak, Dy^{3+} ions are located at an inversion symmetric site, and when yellow light emission due to electric dipole transition is strong, Dy^{3+} ions are located at non-inversion symmetry sites.[31,32] In this study, since the intensity of 572 nm, which is yellow light emission, was stronger than that of 480 nm, which is the blue light emission, the Dy^{3+} ions located in the $BaMoO_4$ crystal were accordingly located in non-inversion symmetry (Fig. 3(a)). Fig. 3(b) shows the absorption and emission spectra of the $BaMoO_4:Sm^{3+}$ phosphor single doped with Sm^{3+} ions. An absorption signal by CTB between Sm^{3+} cations and O^{2-} anions with a wide bandwidth at 230–340 nm and a peak at 286 nm, and several absorption signals at 340–400 nm with a rather narrow bandwidth, were observed. Absorption signals with relatively narrow bandwidths had peaks at 344 ($^6H_{5/2} \rightarrow {}^4K_{17/2}$), 361 ($^6H_{5/2} \rightarrow {}^4H_{7/2}$), and 375 ($^6H_{5/2} \rightarrow {}^6P_{7/2}$) nm due to *f*–*f* transitions, which were generated when they transitioned from $^6H_{5/2}$ in the bottom state of Sm^{3+} ions, respectively.[33] When the $BaMoO_4:Sm^{3+}$ sample was excited at 286 nm, spectra with peaks at 560, 597, 641, and 702 nm were observed. A strong red emission spectrum was exhibited, and these are the peak emission spectra due to the $^4G_{5/2} \rightarrow {}^6H_j$ (j = 5/2, 7/2, 9/2) transition of Sm^{3+}. The yellow and orange fluorescence spectra are magnetic dipole transition signals generated by the $^4G_{5/2} \rightarrow {}^6H_{5/2}$ and $^4G_{5/2} \rightarrow {}^6H_{7/2}$ transitions, and the red fluorescence spectrum is a signal due to the $^4G_{5/2} \rightarrow {}^6H_{9/2}$ electric dipole transition.[34,35] In the synthesized $BaMoO_4:Sm^{3+}$ phosphor, the ratio of the emission intensity of the spectrum emitted by the magnetic dipole transition and the electric dipole transition was relatively strong due to the reddish orange electric dipole transition. In general, it is known that the main emission wavelength intensity produced by rare earth ions is determined by competition between the magnetic dipole transition and electric dipole transition.[36] As in the Dy^{3+}-doped specimen, if the light emission intensity due to magnetic dipole transition is strong, it is located in inversion symmetry. The Sm^{3+} doped

sample also has a stronger luminescence intensity because the red (641 nm) electric dipole transition is greater than that of the orange (597 nm) light emission, so Sm^{3+} ions located in $BaMoO_4$ crystals are located in non-inversion symmetric sites.

3.2. Characteristics of rare earth co-doped $BaMoO_4$

To prepare a white light-emitting phosphor, Dy^{3+} and Sm^{3+} ions were co-doped and synthesized as $BaMoO_4$:[Sm^{3+}]/[Dy^{3+}]. To confirm the crystal structure of the synthesized phosphor, after the pattern according to the Sm^{3+} concentration change X-ray diffraction analysis is shown in Fig. 4(a). The synthesized phosphor was consistent with the ICDD no. 00-008-0455 card, and the tetragonal structure of $BaMoO_4$ was confirmed. A signal on the main peak (112) was strongly detected in the synthesized $BaMoO_4$:[Sm^{3+}]/[Dy^{3+}] phosphor, and (004), (200), (112), (213), (204), (220), (116), (312), (224) phases were observed. The amount of added Dy^{3+} ions was fixed, and as the doping concentration of Sm^{3+} ions increased, a small shoulder was observed on the left side of the main peak (112). From the $BaMoO_4$:[Sm^{3+}]/[Dy^{3+}] $\sim$ 6 sample, a shoulder was observed at the position indicated by diamonds. This was confirmed to be the Sm_2O_3 phase, which appeared due to the excessive doping of Sm^{3+} ions and oxidized rare earth ions. To investigate the particle size and formation of the $BaMoO_4$:[Sm^{3+}]/[Dy^{3+}] phosphor synthesized at room temperature by co-precipitation, FE-SEM imaging was performed, and the image is shown in Fig. 4(b). The synthesized particles of the phosphor powder had a long octahedral shape in the longitudinal direction. The size was about 1.08 μm in the horizontal direction and about 2.63 μm in the longitudinal direction. Muhammad *et al.* synthesized crystalline Co_3O_4 nanoparticles at a temperature of 60 °C in a process like the co-precipitation method used in this study and observed plate-shaped particles of several to several tens of microns using FE-SEM.[37] F. Sedighi *et al.* synthesized silver doped crystalline $SrWO_4$ at 70 °C by co-precipitation to observe the shape of a flower and particles such as a star, and reported a change in the shape of the particles depending on the amount of added $Na(B(C_6H_5))$.[38] Fig. 5(a) illustrates the PL spectrum of the co-doped $BaMoO_4$:[Sm^{3+}]/[Dy^{3+}] phosphor after fixing the concentration of Dy^{3+} ions and adjusting the amount of added Sm^{3+} ions. When the samples were excited at 291 nm, a signal at 572 nm, the main peak of Dy^{3+}, was strongly detected, but the intensity of the signal decreased as the doping concentration of Sm^{3+} ions increased. From the $BaMoO_4$:[Sm^{3+}]/[Dy^{3+}] $\sim$ 0.3 sample, blue light emission at 480 nm ($^4F_{9/2} \rightarrow {}^6H_{15/2}$) and yellow light emission at 572 nm ($^4F_{9/2} \rightarrow {}^6H_{13/2}$) of Dy^{3+} ions, orange light emission at 597 nm ($^4G_{5/2} \rightarrow {}^6H_{7/2}$) and red light emission at 641 nm ($^4G_{5/2} \rightarrow {}^6H_{9/2}$) of Sm^{3+} ions were observed together. As shown in Fig. 5(b), the yellow signal at 572 nm, the main peak of Dy^{3+}, decreased as the concentration of Sm^{3+} ions increased, but the red signal at 641 nm increased. This phenomenon means that the luminescence energy was converted from Dy^{3+} ions located in the $BaMoO_4$, the host crystal, to Sm^{3+} ions. The energy transfer from Dy^{3+} ions to Sm^{3+} ions can be expressed by eqn (1).[39]

$$\eta = 1 - I/I_0 \quad (1)$$

Here, I is the emission intensity of Dy^{3+} ions in the phosphor co-doped with Dy^{3+} and Sm^{3+} ions, and I_0 is the emission intensity of Dy^{3+} ions in the phosphor doped with Dy^{3+} single ions. Fig. 5(c) shows that the energy transfer (ET) efficiency increases sharply from the sample of $BaMoO_4$:[Sm^{3+}]/[Dy^{3+}] $\sim$ 0.6 with the doping concentration of Sm^{3+} ions, and the main peaks are 572 nm and 641 nm. It showed the same result as the change. As the amount of Sm^{3+} doped increased, the PL intensity decreased along with the distance between Sm^{3+} ions. This can be interpreted as a concentration quenching, in which emission intensity decreases due to the non-radiative energy transfer generated between the activator Sm^{3+} ions.[40] Photoexcited rare earth-doped semiconductors suffer from this so-called concentration quenching effect, in which the intensity of the rare earth emission decreases with increasing dopant concentration. This effect is dominant when the excitation energy moves between many ions within the time required for radioactive decay. This is often referred to as energy transfer. In such situations, the chances of reaching a path of non-radioactive decay are greatly increased. Concentration quenching is a typical effect at high concentrations, as the probability of

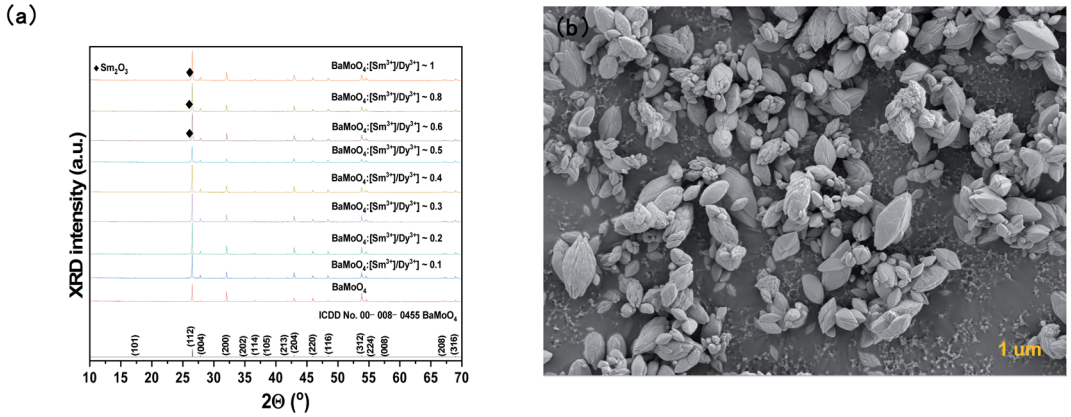

Fig. 4 (a) XRD patterns of $BaMoO_4$:[Sm^{3+}]/[Dy^{3+}] according to Sm^{3+} ion concentration and (b) FE-SEM image of $BaMoO_4$:[Sm^{3+}]/[Dy^{3+}].

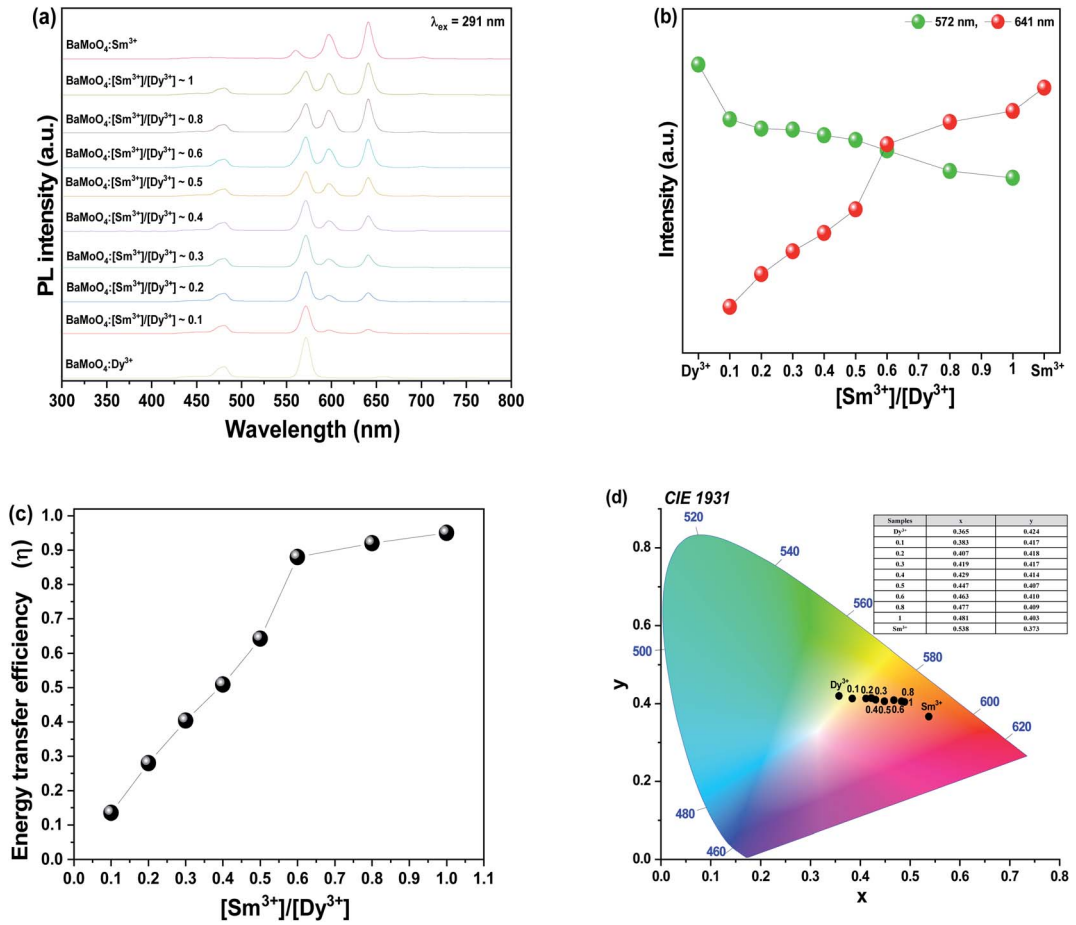

Fig. 5 $BaMoO_4$:$[Sm^{3+}]/[Dy^{3+}]$ of (a) PL spectra under 291 nm, (b) change of 572 nm (Dy^{3+}) and 641 nm (Sm^{3+}), (c) energy transfer efficiency, and (d) CIE coordinate of the $BaMoO_4$ phosphors.

energy transfer increases as the density increases with the decreasing distance between dopants.

The critical distance R_C was calculated using the following equations:[40]

$$R_C \approx 2[3V/4\pi x_c N]^{1/3} \quad (2)$$

where V is the volume of the host unit cell ($V = 399.20$ Å^3), x_c is the total concentration of $[Sm^{3+}]/[Dy^{3+}]$ maximum and minimum intensity ($x_c = 0.1, 1$) and N is the number of host cations in the unit cell ($N = 4$). The critical distance of $[Sm^{3+}]/[Dy^{3+}] \sim 0.1$ was calculated to be 12.40 Å, and at $[Dy^{3+}]/[Ce^{3+}] \sim 1$ was calculated to be 5.755 Å. These results indicate that concentration quenching occurs when the distance between the activator ions Sm^{3+} and Dy^{3+} approached. There are three types of well known interactions in which the electric multipolar interaction is involved in the energy transfer: dipole–dipole, dipole–quadrupole, and quadrupole–quadrupole interactions.[41] Fig. 5(d) shows the CIE (Commission Internationale de L'Eclairage) color coordinates of the synthesized phosphors, $BaMoO_4$:Dy^{3+}, $BaMoO_4$:Sm^{3+}, and $BaMoO_4$:$[Sm^{3+}]/[Dy^{3+}]$. The $BaMoO_4$:Dy^{3+} phosphor was in yellow with coordinates (0.365, 0.424) and the $BaMoO_4$:Sm^{3+} phosphor was located in the orange position with coordinates (0.538, 0.373). The $BaMoO_4$:$[Sm^{3+}]/[Dy^{3+}]$ phosphor moved from yellow to white through red as the doping concentration of Sm^{3+} ions increased, and the emission color of the phosphor could be controlled by the doping concentration of rare earth ions. The energy level structure of Dy^{3+} and Sm^{3+} as shown in Fig. 6. The electrons located at the ground state $^6H_{15/2}$ of Dy^{3+} ion absorb energy under 291 nm excitation energy and later jump to the excited state. Since the high energy level is unstable, these electrons will drop successively to the lower energy excited state $^4F_{9/2}$ by non-radiative transition (NR). With the populated $^4F_{9/2}$ level, the radiative transitions of Dy^{3+} occurred with yellow and blue emissions due to the $^4F_{9/2} \rightarrow {}^6H_{15/2}$, $^6H_{13/2}$, $^6H_{11/2}$ transitions, respectively. In the interim, partial electrons located at the $^4F_{9/2}$ level of Dy^{3+} are relaxed to the $^6H_{5/2}$ level of Sm^{3+} by the resonance between the two levels, which ultimately gives rise to the characteristic emissions of Sm^{3+}.[42]

3.3. Flexible composite for LED color filter

When the synthesized $BaMoO_4$:Dy^{3+}, $BaMoO_4$:Sm^{3+}, $BaMoO_4$:$[Sm^{3+}]/[Dy^{3+}] \sim 0.1$ phosphor powder was placed under a UV lamp, yellow, white, and reddish orange emission colors could be observed as shown in Fig. 7. The $BaMoO_4$:Dy^{3+} phosphor showed a yellow emission wavelength, but green emission was seen in photography. It looked yellowish close to white with the naked

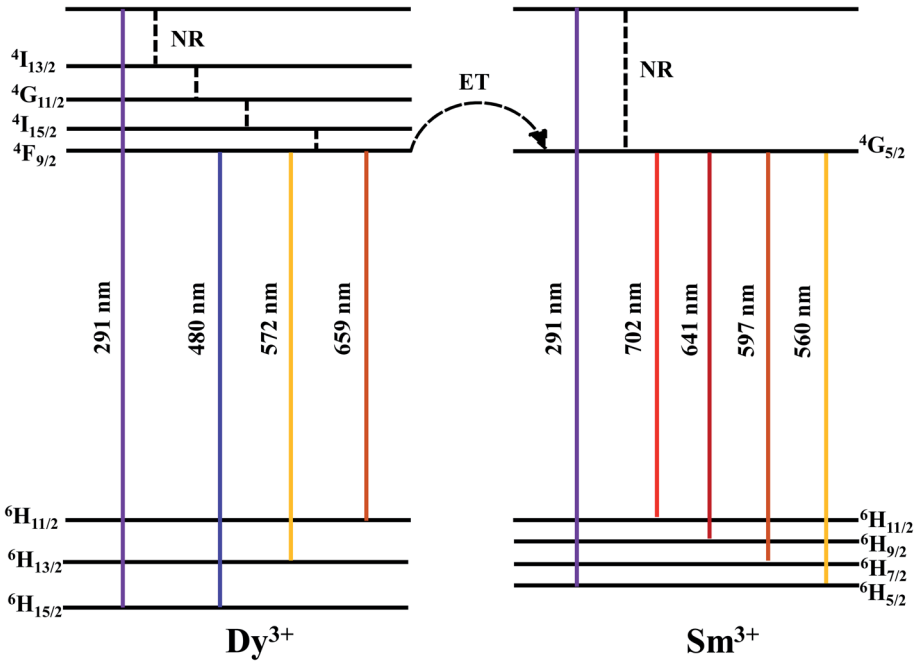

Fig. 6 Schematic energy level structure of the Dy^{3+} and Sm^{3+} ions.

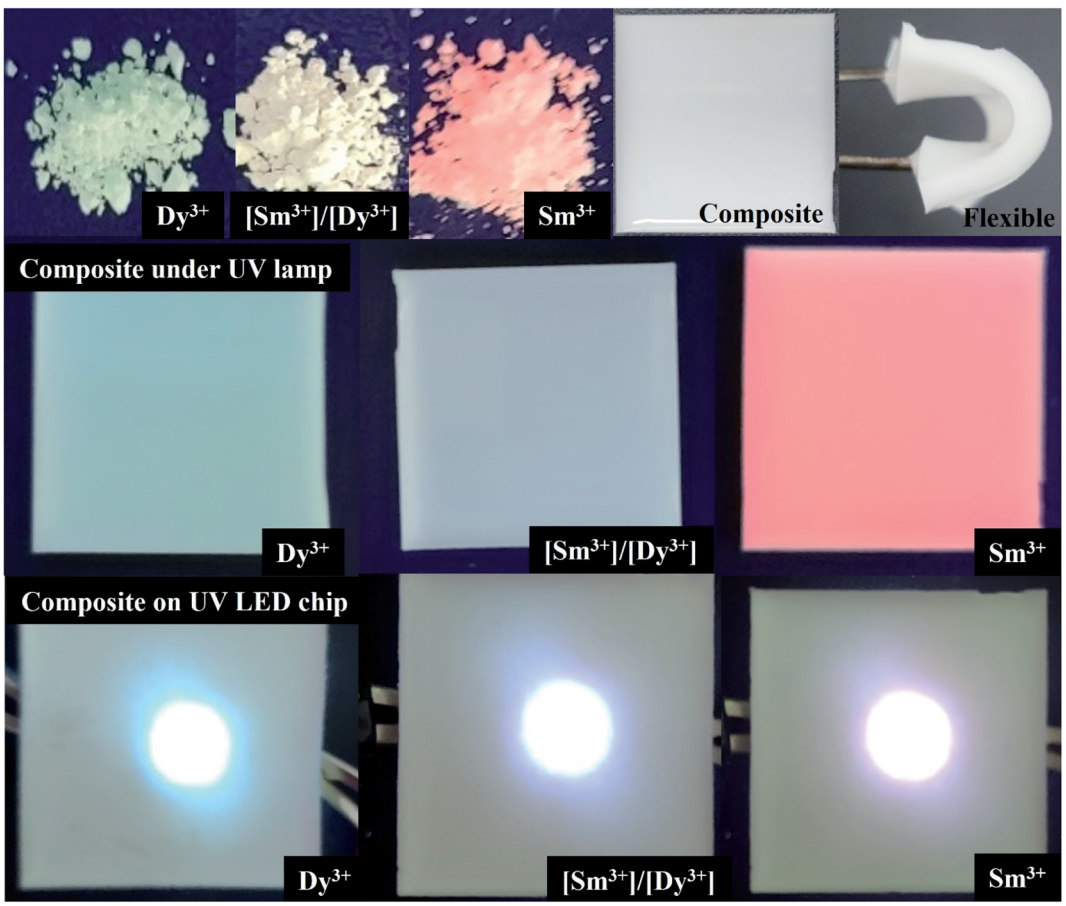

Fig. 7 Photographs of synthesized phosphors powder and flexible composite under UV lamp, and composite applied on the UV-LED chip.

eye, but it was photographed as green due to a camera filter. Composites were made by mixing individual powders with PDMS, a silicon-based polymer, which were easily bent and exhibited a unique color emission like that of the powder. To determine whether the manufactured composite could be used as an LED filter, a voltage of about 10 V was applied to the LED chip by placing the composite on a UV-LED chip. The manufactured composite exhibited colors similar to those in UV lamps, and this suggests that the $BaMoO_4$ phosphor synthesized by doping with rare earth ions could be used as an LED color filter.

4. Conclusion

Crystalline $BaMoO_4$ was synthesized at room temperature by co-precipitation. Using the $BaMoO_4$ as a phosphor host, Dy^{3+} and Sm^{3+}, which are rare earth ions, were doped to synthesize the phosphor. Diffraction analysis confirmed a tetragonal structure, and a strong diffraction peak on the main peak (112). After doping with rare earth ions with relatively large ionic radii, the lattice constant of the (112) phase and the position of the Raman signal were changed. $BaMoO_4$:Dy^{3+} and $BaMoO_4$:Sm^{3+} phosphors excited with UV wavelengths with strong absorbance in the UV region showed yellow and reddish orange spectra. A sample was prepared, $BaMoO_4$:[Sm^{3+}]/[Dy^{3+}], by co-doping with Dy^{3+} and Sm^{3+} ions for white light fluorescence, and the main peak (112) phase was also confirmed by X-ray diffraction analysis. However, as the concentration of Sm^{3+} ions was increased, a secondary phase Sm_2O_3 peak was observed. When the sample was excited at 291 nm, the intensity of the reddish orange emission spectrum in the yellow emission spectrum increased, as the concentration of Sm^{3+} ions increased. The synthesized phosphor, $BaMoO_4$:[Sm^{3+}]/[Dy^{3+}] $\sim$ 0.1 showed white light emission, and a composite was prepared by mixing it with a PDMS polymer for use as an LED color filter. The prepared composite was easily bent, and when applied on a UV-LED chip, the light emission of yellow, white, and reddish orange, which are the intrinsic colors of the synthesized phosphor, were confirmed.

Data availability statement

The data presented in this study are available on request from the corresponding author.

Conflicts of interest

The authors declare no conflict of interest.

Acknowledgements

This research was supported by Basic Science Research Program through the National Research Foundation of Korea (NRF) funded by the Ministry of Education (NRF-2020R1F1A1072676).

References

1 G. B. Nair, H. C. Swart and S. J. Dhoble, *Prog. Mater. Sci.*, 2020, **109**, 100622, DOI: 10.1016/j.pmatsci.2019.100622.
2 G. Li, N. Yang, J. Zhang, J. Si, Z. Wang, G. Cai and X. Wang, *The Non-Concentration-Quenching Phosphor $Ca_3Eu_2B_4O_{12}$ for WLED Application*, American Chemical Society (ACS), 2020.
3 H. Kuo, C. Hung, H. Chen, K. Chen, C. Wang, C. Sher, C. Yeh, C. Lin, C. Chen and Y. Cheng, *Opt. Express*, 2011, **19**(4), A930–A936, DOI: 10.1364/OE.19.00A930.
4 N. T. Tran and F. G. Shi, *J. Lightwave Technol.*, 2008, **26**, 3556–3559, DOI: 10.1109/JLT.2008.917087.
5 Y. Lin, M. Karlsson and M. Bettinelli, *Top. Curr. Chem.*, 2016, **374**, 21, DOI: 10.1007/s41061-016-0023-5.
6 L. Yang, Z. Mu, S. Zhang, Q. Wang, D. Zhu, Y. Zhao, D. Luo, Q. Zhang and F. Wu, *J. Mater. Sci.: Mater. Electron.*, 2018, **29**, 6548–6555, DOI: 10.1007/s10854-018-8638-7.
7 S. Zhang, H. Liu, D. Pan, J. Tian, Y. Liu and A. A. Volinsky, *RSC Adv.*, 2014, **5**, 1113–1119, DOI: 10.1039/c4ra12879f.
8 R. P. Sreekanth Chakradhar, B. M. Nagabhushana, G. T. Chandrappa, K. P. Ramesh and J. L. Rao, *J. Chem. Phys.*, 2004, **121**, 10250–10259, DOI: 10.1063/1.1808420.
9 C. Xiangzhong, Z. Weidong, Z. Xiying, X. Tian, L. Zhen, Y. Zhijian, Z. Chunlei and H. Xiaowei, *Red Emitting Phosphor (Y, Gd)BO_3:Eu^{3+} for PDP Prepared by Complex Method*, Elsevier BV, 2006.
10 I. P. Sahu, D. P. Bisen and N. Brahme, *Luminescence*, 2015, **30**, 526–532, DOI: 10.1002/bio.2771.
11 L. Jiang, C. Chang, D. Mao and B. Zhang, *Mater. Lett.*, 2004, **58**, 1825–1829, DOI: 10.1016/j.matlet.2003.11.014.
12 L. Han, G. Liu, X. Dong, J. Wang, X. Wang and Y. Yang, *J. Mater. Sci.: Mater. Electron.*, 2017, **28**, 16519–16526, DOI: 10.1007/s10854-017-7564-4.
13 G. Dominiak-Dzik, W. Ryba-Romanowski, R. Lisiecki, P. Solarz, B. Macalik, M. Berkowski, M. Głowacki and V. Domukhovski, *Cryst. Growth Des.*, 2010, **10**, 3522–3530, DOI: 10.1021/cg100429b.
14 L. Zur, *J. Mol. Struct.*, 2013, **1041**, 50, DOI: 10.1016/j.molstruc.2013.02.036.
15 G. Raju, J. Y. Park, H. C. Jung, H. K. Yang, B. K. Moon, J. H. Jeong and J. H. Kim, *Opt. Mater.*, 2009, **31**, 1210–1214, DOI: 10.1016/j.optmat.2008.12.015.
16 J. Kuang, Y. Liu and J. Zhang, *J. Solid State Chem.*, 2006, **179**, 266–269, DOI: 10.1016/j.jssc.2005.10.025.
17 L. Li, W. Zi, G. Li, S. Lan, G. Ji, S. Gan, H. Zou and X. Xu, *J. Solid State Chem.*, 2012, **191**, 175–180, DOI: 10.1016/j.jssc.2012.03.003.
18 B. Fan, J. Liu, W. Zhao and L. Han, *J. Lumin.*, 2020, **219**, 116887, DOI: 10.1016/j.jlumin.2019.116887.
19 X. Yu, X. Xu and J. Qiu, *Mater. Res. Bull.*, 2011, **46**, 627–629, DOI: 10.1016/j.materresbull.2010.12.028.
20 V. Nassif, R. E. Carbonio and J. A. Alonso, *J. Solid State Chem.*, 1999, **146**, 266–270, DOI: 10.1006/jssc.1999.8352.
21 J. Jung, J. Kim, Y. Shim, D. Hwang and C. S. Son, *Materials*, 2020, **13**, 4165, DOI: 10.3390/ma13184165.
22 T. Thongtem, S. Kungwankunakorn, B. Kuntalue, A. Phuruangrat and S. Thongtem, *J. Alloys Compd.*, 2010, **506**, 475–481, DOI: 10.1016/j.jallcom.2010.07.033.
23 C. G. Pope, *J. Chem. Educ.*, 1997, **74**, 129, DOI: 10.1021/ed074p129.

24 F. Boulc'h and E. Djurado, *Solid State Ionics*, 2003, **157**, 335–340, DOI: **10.1016/S0167-2738(02)00230-8**.
25 F. F. Sene, J. R. Martinelli and L. Gomes, *J. Non-Cryst. Solids*, 2004, **348**, 63–71, DOI: **10.1016/j.jnoncrysol.2004.08.127**.
26 V. Panchal, N. Garg and S. M. Sharma, *J. Phys.: Condens. Matter*, 2006, **18**, 3917–3929, DOI: **10.1088/0953-8984/18/16/002**.
27 M. Guo, J. Lu, Y. Wu, Y. Wang and M. Luo, *Langmuir*, 2011, **27**, 3872–3877, DOI: **10.1021/la200292f**.
28 B. Vengala Rao, K. Jang, Ho S. Lee, S. Yi and J. Jeong, *J. Alloys Compd.*, 2010, **496**, 251–255, DOI: **10.1016/j.jallcom.2009.12.175**.
29 F. Zhang, Y. Wang, Y. Wen, D. Wang and Y. Tao, *Opt. Mater.*, 2011, **33**, 475–479, DOI: **10.1016/j.optmat.2010.10.035**.
30 K. Mishra, S. K. Singh, A. K. Singh and S. B. Rai, *Mater. Res. Bull.*, 2012, **47**, 1339–1344, DOI: **10.1016/j.materresbull.2012.03.017**.
31 S. Liu, S. Liu, J. Wang, P. Sun, Y. Zhong, J. H. Jeong, B. Deng and R. Yu, *Mater. Res. Bull.*, 2018, **108**, 275–280, DOI: **10.1016/j.materresbull.2018.08.026**.
32 Y. Tian, B. Chen, B. Tian, R. Hua, J. Sun, L. Cheng, H. Zhong, X. Li, J. Zhang, Y. Zheng, T. Yu, L. Huang and Q. Meng, *J. Alloys Compd.*, 2011, **509**, 6096–6101, DOI: **10.1016/j.jallcom.2011.03.034**.
33 M. Kumar and A. S. Rao, *Opt. Mater.*, 2020, **109**, 110356, DOI: **10.1016/j.optmat.2020.110356**.
34 M. P. Demesh, O. P. Dernovich, N. V. Gusakova, A. S. Yasukevich, A. A. Kornienko, E. B. Dunina, L. A. Fomicheva, A. A. Pavlyuk and N. V. Kuleshov, *Opt. Mater.*, 2018, **75**, 821–826, DOI: **10.1016/j.optmat.2017.12.001**.
35 L. Liu, J. Zhang, F. Xu, F. Du, F. Yang, J. Peng and X. Ye, *J. Rare Earths*, 2021, **39**, 140–145, DOI: **10.1016/j.jre.2020.03.004**.
36 G. Phaomei, W. Rameshwor Singh and R. S. Ningthoujam, *J. Lumin.*, 2011, **131**, 1164–1171, DOI: **10.1016/j.jlumin.2011.02.023**.
37 J. Muhammad Ramzan Saeed Ashraf, *Open Chem.*, 2019, **17**, 865–873, DOI: **10.1515/chem-2019-0100**.
38 F. Sedighi, A. Sobhani-Nasab, M. Esmaeili-Zare and M. Behpour, *J. Nanostruct.*, 2019, **9**, 331–339, DOI: **10.22052/JNS.2019.02.015**.
39 N. Liu, L. Mei, L. Liao, J. Fu and D. Yang, *Sci. Rep.*, 2019, **9**, 1–9, DOI: **10.1038/s41598-019-51915-1**.
40 V. R. Kharabe, A. H. Oza and S. J. Dhoble, *Luminescence*, 2015, **30**, 432–438, DOI: **10.1002/bio.2756**.
41 B. Bondzior, D. Stefańska, A. Kubiak and P. J. Dereń, *J. Lumin.*, 2017, **190**, 123–127, DOI: **10.1016/j.jlumin.2017.05.017**.
42 C. Chen, C. Yu, F. Xu, Q. Li and Y. Zhang, *Ceram. Int.*, 2021, **47**, 1–9, DOI: **10.1016/j.ceramint.2020.08.190**.